Neural Stimulation and Recording with Bidirectional, Soft Carbon Nanotube Fiber Microelectrodes

Flavia Vitale,[†] Samantha R. Summerson,[‡] Behnaam Aazhang,[§] Caleb Kemere,[§] and Matteo Pasquali*[,†,∥]

[†]Department of Chemical and Biomolecular Engineering, Rice University, Houston, Texas 77005, United States, [‡]Department of Electrical Engineering and Computer Sciences and Helen Wills Neuroscience Institute, University of California, Berkeley, California 94720, United States, [§]Department of Electrical and Computer Engineering, Rice University, Houston, Texas 77005, United States, and [∥]Department of Chemistry, Department of Material Science & NanoEngineering, and The Smalley Institute for Nanoscale Science & Technology, Rice University, Houston, Texas 77005, United States

ABSTRACT The development of microelectrodes capable of safely stimulating and recording neural activity is a critical step in the design of many prosthetic devices, brain–machine interfaces, and therapies for neurologic or nervous-system-mediated disorders. Metal electrodes are inadequate prospects for the miniaturization needed to attain neuronal-scale stimulation and recording because of their poor electrochemical properties, high stiffness, and propensity to fail due to bending fatigue. Here we demonstrate neural recording and stimulation using carbon nanotube (CNT) fiber electrodes. *In vitro* characterization shows that the tissue contact impedance of CNT fibers is remarkably lower than that of state-of-the-art metal electrodes, making them suitable for recording single-neuron activity without additional surface treatments. *In vivo* chronic studies in parkinsonian rodents show that CNT fiber microelectrodes stimulate neurons as effectively as metal electrodes with 10 times larger surface area, while eliciting a significantly reduced inflammatory response. The same CNT fiber microelectrodes can record neural activity for weeks, paving the way for the development of novel multifunctional and dynamic neural interfaces with long-term stability.

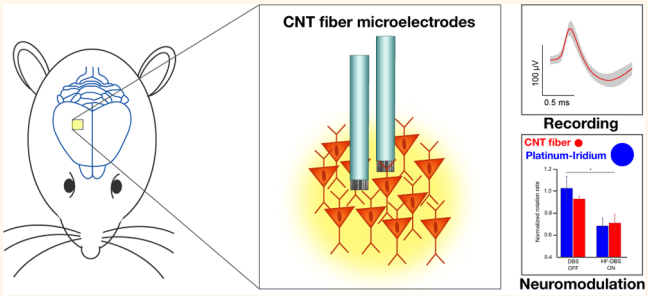

KEYWORDS: neural interfaces · soft neural microelectrodes · carbon nanotube fibers · multifunctional microelectrodes · ultrasmall neural probes · long-term recordings · single-neuron isolation · deep brain stimulation · brain–machine interfaces

Electrical stimulation of neural activity is the basis of a number of technologies for the restoration of sensory or motor functions,[1−4] brain–machine interfaces (BMI),[5,6] deep brain stimulation (DBS) therapies for neurological disorders (*i.e.*, DBS for Parkinson's disease (PD), dystonia, and depression),[7] and peripheral nerve stimulation for treatment of a variety of diseases.[8] In all of these applications, the electrode is the essential component that connects the man-made device with the nervous system by delivering the charge required to initiate a functional response in the neural structures. Stimulating electrodes must deliver the necessary amount of charge without exceeding the safety voltage limits while remaining stable, functional, and biocompatible for chronic use. Moreover, a requirement of a number of emerging applications is an interface that establishes bidirectional communications with neural ensembles, which dictates the use of electrodes on the size scale of individual neurons,[9] that is, geometric surface areas below ∼2000 μm^2. Metal microelectrodes suffer from intrinsic limitations in the maximum current and charge density that can be delivered through capacitive or reversible faradaic mechanisms. Moreover, the high impedance of metal microelectrodes degrades the signal-to-noise ratio (SNR) and sensitivity of recordings. Finally, the mechanical mismatch between stiff metals and soft brain tissue causes inflammation and scarring, neuronal degeneration, and loss of recording functionality in chronic use.[10,11]

Metallic and organic coatings on the electrode active site, such as poly(3,4-ethylenedioxythiophene) (PEDOT)[12,13] and iridium oxide (IrOx),[14] have been shown to improve charge transfer and impedance

* Address correspondence to mp@rice.edu.

Received for review February 14, 2015 and accepted March 24, 2015.

Published online March 24, 2015
10.1021/acsnano.5b01060

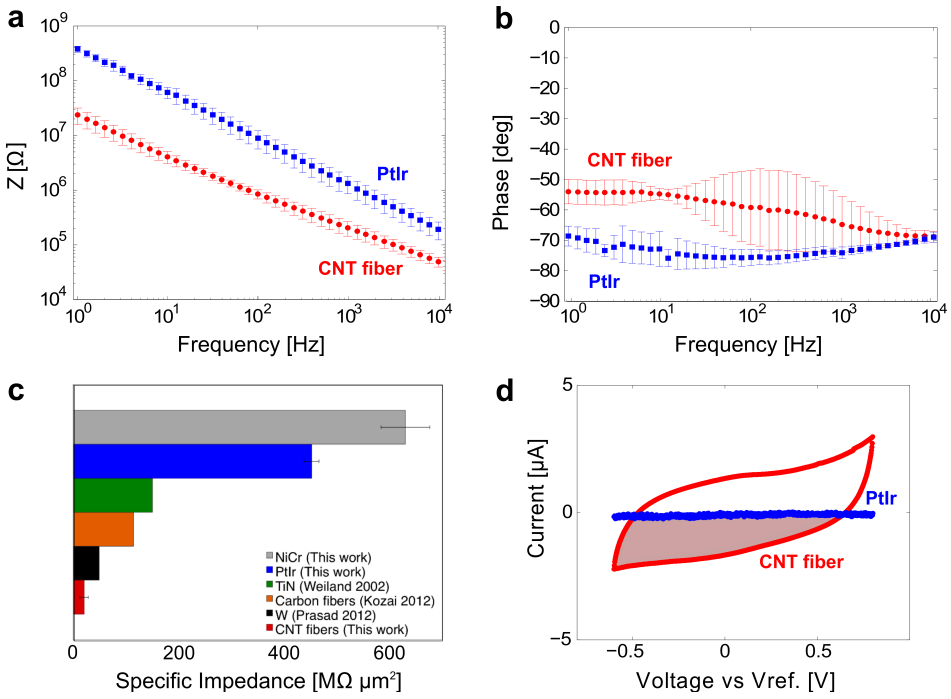

Figure 1. ***In vitro*** **characterization of CNT fiber microelectrode properties and comparison with other electrode materials. (a) Modulus and (b) phase of the impedance of CNT fiber and PtIr wires (diameter: 18 μm, $n = 5$); (c) specific impedance at 1 kHz; (d) cyclic voltammetry of CNT fiber and PtIr electrodes used for *in vivo* DBS study. The shaded area is used to calculate cathodic charge storage capacity of the electrodes.**

properties. However, degradation and delamination of the coating materials still greatly limit electrode longevity and, thus, their chronic use.[12,15,16] Recently, carbon fibers have been used to fabricate subcellular scale size microelectrodes (4.5 to 7 μm in diameter) with improved performance in terms of biocompatibility and quality of chronic *in vivo* recordings.[13,17] However, the high impedance and low charge injection of carbon fibers[13] make them unsuitable for chronic applications in neural stimulation.

Carbon nanotubes (CNTs) have attracted increasing attention, due to the intrinsically high mass-specific surface area,[18] mechanical strength,[19] electrical conductivity,[20] and biological stability.[21] Moreover, Poulin *et al.* demonstrated that microelectrodes made solely of CNT fibers[22] show remarkable electrochemical activity, sensitivity, and resistance to biofouling compared to conventional carbon fibers when used for bioanalyte detection *in vitro*.[23−25] However, despite some promising initial attempts,[26−30] the feasibility, scalability, *in vivo* performance, and long-term stability of CNT-based electrodes have not yet been demonstrated.

Here we show that high-performance CNT fibers[31] possess remarkable electrochemical properties, yield electrodes combining small surface area, low impedance, effective therapeutic stimulation, long-term stability, and biocompatibility, and can be used to reliably detect and isolate single neuronal units over several weeks.

RESULTS AND DISCUSSION

Electrochemical Characterization. Electrodes were fabricated by insulating individual CNT fibers[31] with a ~3 μm layer of a copolymer of polystyrene−polybutadiene (PS-*b*-PBD), leaving only the tip exposed as an electrically active site. PS-*b*-PBD was selected because of good dielectric properties, biocompatibility, flexibility, and resistance to flexural fatigue.[32] Electrochemical properties of the resultant electrodes were characterized through analysis of impedance, charge storage capacity, charge injection limit, and the water window. While specific requirements depend on the application, minimization of impedance and maximization of the charge storage and injection properties are generally considered particularly desirable to achieve noise reduction and stability of recordings and safety and efficacy of stimulation.[9] Electrochemical impedance spectroscopy (EIS) shows that the impedance of the CNT fiber microelectrode is 15 to 20 times lower than that of a PtIr wire of the same size (18 μm diameter, Figure 1a) in the range of frequencies tested (1 Hz to 10 kHz)—the specific impedance at 1 kHz is also 2.5 to 6 times better than tungsten[33] and carbon fibers[13] (Figure 1c). The improved impedance arises from the high surface area of CNT fibers accessible to ions due to the interstitial spaces between the aligned CNTs and CNT bundles constituting the fiber.[31] The impedance phase lag and the featureless appearance of the cyclic voltammogram (Figure 1b,d) indicate that

TABLE 1. Mechanical and Electrical Properties of CNT Fiber and PtIr Stimulating Microelectrodes

	exposed active site surface area (μm^2)	specific impedance (MΩ μm^2)	charge storage capacity (mC/cm^2)	charge injection limit (mC/cm^2)	axial stiffness (N/m)	lateral stiffness (N/m)
CNT fibers	1450	20.44 $\pm$ 8.2	372 $\pm$ 56	6.52	5.09 $\times$ 10^3	0.02
PtIr	17000	451.9 $\pm$ 13.9	1.2 $\pm$ 0.08	0.15	1.3 $\times$ 10^5	0.77

the electrochemical interaction is controlled by capacitive charging and discharging of the CNT fiber–electrolyte double layer; this is particularly advantageous for neural stimulation because it avoids the risk of tissue damage from irreversible faradaic reactions.[9] Moreover, the cathodic charge storage capacity (shaded area in Figure 1d), which characterizes the maximum charge available for stimulation, is 372 $\pm$ 56 mC/cm^2, 2–3 orders of magnitude higher than other materials.[34−36] One of the main limitations of stimulating metal electrodes is the low charge density that can be delivered during a stimulation pulse without exceeding the water electrolysis limits. CNT fibers show a wide water window, with the reduction and oxidation potentials of −1.5 and 1.5 V, respectively (Supporting Information Figure S1); the charge injection capacity calculated from the voltage excursion at a conservative maximum negative potential of −1 V is 6.5 mC/cm^2, more than two times higher than typical electrode materials.[34−36] In standard electrode design, high interface impedance and low charge injection capacity are usually mitigated by using electrically active coatings (such as PEDOT), which might degrade under overpulsing conditions.[12,15,16] Conversely, CNT fibers are stable even when subjected to 97M cycles of pulsing beyond the water window limits (9 days), whereas PEDOT coatings fail after 43M cycles (Supporting Information Figure S2). We fabricated CNT fiber microelectrodes with active site surface area of 1450 μm^2, impedance of 11.2 $\pm$ 7.6 kΩ, and estimated stiffness in the direction perpendicular and lateral to the active site of 6.1 kN/m and 12 mN/m, respectively (Table 1 and Figure 2a). As a comparison, commercial PtIr stimulating microelectrodes have an active site of 17 000 μm^2, impedance of 37.9 $\pm$ 14 kΩ, and more than 1 order of magnitude higher axial and lateral stiffness (Table 1 and Figure 2b–d).

Surgical Implantation and *In Vivo* Stimulation Efficacy of CNT Fiber Microelectrodes. The substantially smaller size and increased flexibility of CNT fiber microelectrodes compared with typical metal electrodes of equivalent impedance suggests that they should be significantly more biocompatible. However, are CNT fiber stimulating electrodes functional? To assess functionality and biocompatibility, we compared CNT fiber and commercial stimulating PtIr electrodes in an experimental model of deep brain stimulation for Parkinson's disease. Four rats were injected with the neurotoxin 6-hydroxydopamine (6-OHDA) in the medial forebrain bundle (MFB), resulting in a unilateral loss of dopamine neurons, which models Parkinson's disease on the side of the body contralateral to the lesion.[37] CNT fiber stimulating electrodes were implanted in the ipsilateral entopenducular (EP) nucleus, a stimulation target we have previously validated (Figure 3a).[38] In order to ensure precise implantation in the EP (insertion depth ~8 mm), CNT fiber microelectrodes were implanted using a polyimide shuttle (100 μm diameter) attached with water-soluble poly(ethylene oxide) (PEO). Within a few minutes from implantation, the PEO coating dissolved and the shuttle was removed, leaving the electrode in place (Figure 3c). Inactive PtIr electrodes were implanted in the contralateral EP and used as controls for biocompatibility studies (Figure 3b). The efficacy of the CNT fiber microelectrodes was assayed with a rotation test after methamphetamine administration, which is a commonly adopted behavioral test used to quantify the effectiveness of the DBS treatment

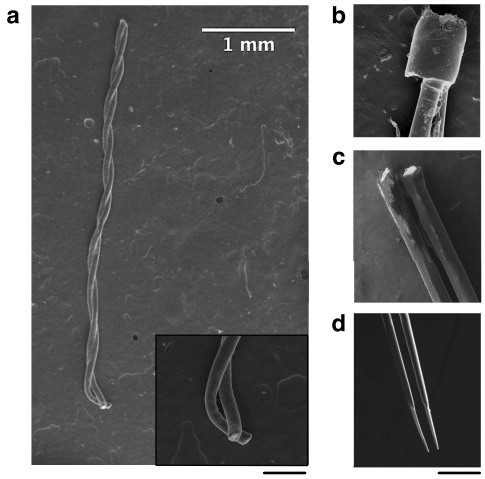

Figure 2. Scanning electron microscopy imaging of CNT fiber and PtIr bipolar microelectrodes used for *in vivo* DBS and biocompatibility study: (a) two-channel CNT fiber microelectrodes, fabricated by twisting single filaments of a 43 μm diameter CNT fiber, coated with a 3 μm layer of PS-*b*-PBD; inset shows a close view of the active site with an average impedance of 11.2 $\pm$ 7.6 kΩ obtained by exposing CNT fibers only at the electrode tip (value expressed as mean $\pm$ SD; scale bar 200 μm). (b–d) PtIr electrode at three different locations: (b) top part of the electrode is composed of a polyimide insulating tube with a length of ~4 cm and a diameter of 200 μm; (c) final 5 mm of the electrode is composed of 75 μm shafts coated with a 3 μm thick layer of parylene. The shafts terminate with (d) tapered active sites with an impedance of 37.9 $\pm$ 7.6 kΩ obtained by exposing 200 μm of PtIr (scale bar 200 μm).

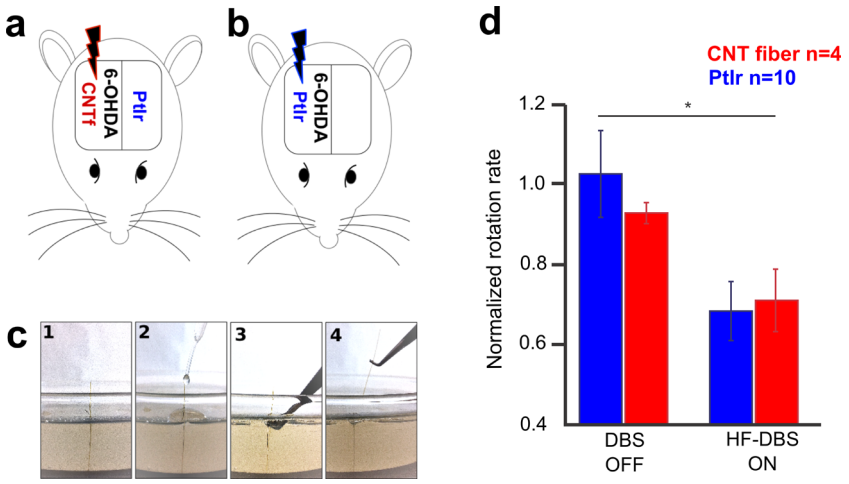

Figure 3. *In vivo* **characterization of efficacy of DBS with CNT fiber microelectrodes. (a,b) Schematic representation of location of the implants for the** *in vivo* **study. 6-OHDA dopaminergic lesion was induced in the MFB of the right hemisphere; (a) CNT fiber microelectrodes or (b) PtIr microelectrodes were implanted ipsilateral to the lesion and used for DBS. In the subjects with CNT fiber implants, inactive commercial PtIr electrodes were implanted contralaterally and used as controls for biocompatibility studies. (c) Illustration of the implant strategy of CNT fibers in 0.6% agar phantom: CNT fiber microelectrode was attached to the PI stiffener with PEO adhesive. From left to right: the stiffener allows the insertion of the CNT fiber in the target area. The PEO adhesive dissolved within a few minutes from the implantation, allowing the removal of the stiffener, while the CNT fiber microelectrode was left in place. (d) Results of the methamphetamine rotation test: average normalized rotation rate of a population of four Long-Evans rats implanted with CNT fiber microelectrodes in comparison with a population of 10 Long-Evans rats implanted with PtIr electrodes. The high-frequency DBS (HF-DBS) condition represents data pooled from stimulation at two high frequencies, 160 and 175 Hz. Repeated measures with ANOVA showed that there was a significant different between treatment conditions ($p < 0.05$). Error bars: ±SD.**

in attenuating the motor asymmetry produced by the unilateral 6-OHDA lesion.[37,38] Effective DBS reduces the unilateral rotation rate, thus demonstrating therapeutic efficacy. DBS with CNT fiber microelectrodes significantly reduced the methamphetamine-induced rotation rate (Figure 3d), confirming that CNT fiber microelectrodes were able to deliver effective stimulation charge in the target EP, with an effect comparable to that of the much larger PtIr electrodes used in our previous study.[38] Thus, the efficacy of CNT fibers in alleviating motor symptoms of PD demonstrate that small, flexible CNT fiber microelectrodes can be precisely implanted in deep brain structures and selectively deliver the stimulation charge needed to elicit therapeutic benefits.

Chronic Biocompatibility and Stability. To assess *in vivo* biocompatibility and stability of CNT fiber microelectrodes, we evaluated both the brain tissue and electrodes 6 weeks postimplantation. In immunohistochemical analysis of the brain hemisphere implanted with CNT fiber microelectrodes, we observed an overall reduction in the extent of the central nervous system specific inflammatory response (*i.e.*, gliosis) and in the expression of inflammatory macrophage phenotypes compared with the PtIr electrode hemisphere (Figure 4). Specifically, we measured a 4-fold reduction in the accumulation of astrocytes and a 2-fold reduction in the expression of general microglia at the CNT fiber microelectrode site (Figure 4a–c). Expression of activated macrophages was found to be confined within approximately 50 μm from CNT fiber microelectrodes and to be more than two times lower than at the PtIr site, where the region of activation extended to more than 150 μm (Figure 4a,d).

Depending on the nature and on the time course of the injury, activated microglia/microphage can differentiate into predominantly "pro-inflammatory" phenotype M-1 or into "anti-inflammatory" phenotype M-2.[39−41] The upregulation of M-1 macrophage expression has been correlated with neurotoxic inflammatory processes, whereas upregulation of M-2 expression is indicative of tissue repair processes, including formation of a fibrotic scar.[41] When stained for surface markers of M-1 and M-2 macrophages, a very low upregulation of both phenotypes could be observed at the site of the CNT fiber implant; conversely, an evident increase was found around the PtIr electrodes, particularly in the case of the M-2 phenotype (Figure 4e,f). These results suggest the presence of an extended fibrotic scar around the PtIr electrode, which is also consistent with the enhanced expression of astrocytes and general microglia. When the tissue was stained for healthy neuronal nuclei, however, a weaker neuronal population was found around the CNT fiber microelectrodes. The zone of neurodegeneration was two times more extended compared to PtIr implants (Figure 4g). We hypothesize that this enhanced neuronal loss was caused by the stiffening shuttle used during the electrode implant procedure.[42,43]

In scanning electron microscopy images of explanted devices, we noted negligible tissue on CNT fiber microelectrodes, in contrast with substantial

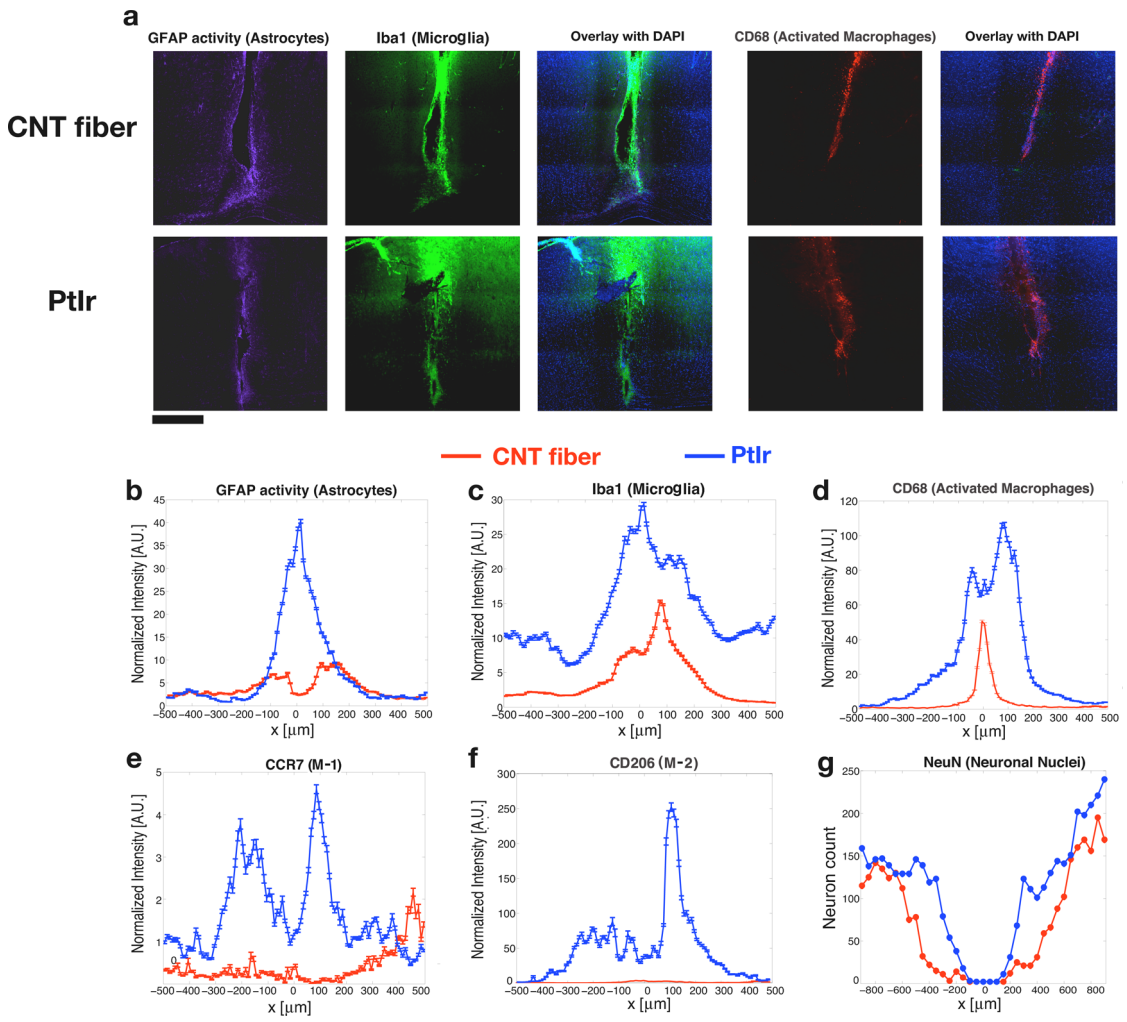

Figure 4. Histological analysis of tissue response to chronic implants of CNT fiber and PtIr electrodes. (a) Fluorescence images of tissue response after 6 weeks of implant with CNT fiber, also used for DBS, and a PtIr electrode implanted contralaterally. Panels show tissue labeled for (from left to right) astrocytes, microglia, and activated macrophages. Scale bar 500 μm. (b–f) Fluorescence intensity profiles at increasing lateral distance *x* from electrode midline: (b) astrocytes, (c) microglia, (d) activated macrophages, (e) "pro-inflammatory" macrophages, (f) "anti-inflammatory" macrophages. Error bar: SD. (g) Neuronal count at increasing lateral distance from the electrode tract.

encapsulation around PtIr implants, which is consistent with results of chronic histology (Supporting Information Figure S3). Additionally, we found no evidence of alterations in the structure of the CNT fibers, no signs of degradation at the stimulation site, and no cracks in the insulation material.

Chronic Recordings of Neural Activity. The small CNT fiber microelectrodes are effective for stimulation. Does lower impedance and biocompatibility translate to quality neural recordings? *In vivo* chronic recording capabilities of CNT fiber microelectrodes were tested in primary motor cortex (M1) of freely behaving rats. The primary motor cortex is the area of the brain that controls the initiation of voluntary movements and is a common target for investigation on neurally controlled prosthetic devices,[3] BMI,[5] and on closed-loop intracortical[5,6] and deep brain stimulation protocols.[44] CNT fiber recording electrodes were fabricated using 12.6 μm individual filaments insulated by PS-*b*-PBD coating. The average impedance of each electrode measured at 1 kHz was 151 $\pm$ 75 kΩ. Four-channel electrode arrays (tetrodes) were fabricated by assembling one CNT fiber microwire with three NiCr wires of the same size (diameter 12 μm). The active site of NiCr electrodes was coated with colloidal gold through galvanostatic deposition (hereafter referred to as NiCr-Au) to reduce the impedance from 3.89 $\pm$ 0.40 MΩ to 250.4 $\pm$ 14.8 kΩ (NiCr-Au is the standard material for multichannel microwire electrodes for *in vivo* electrophysiological recording).[45] The tetrodes were loaded into a microdrive and implanted into M1; after 2 weeks postop recovery, recording experiments were performed every 1 to 2 days on freely behaving animals for the following 2 weeks. We were able to detect and isolate single-unit spikes on CNT fiber electrodes with amplitude and SNR ~3, which is comparable to neighboring NiCr-Au channels, as shown by electrophysiological recordings in the high-frequency range

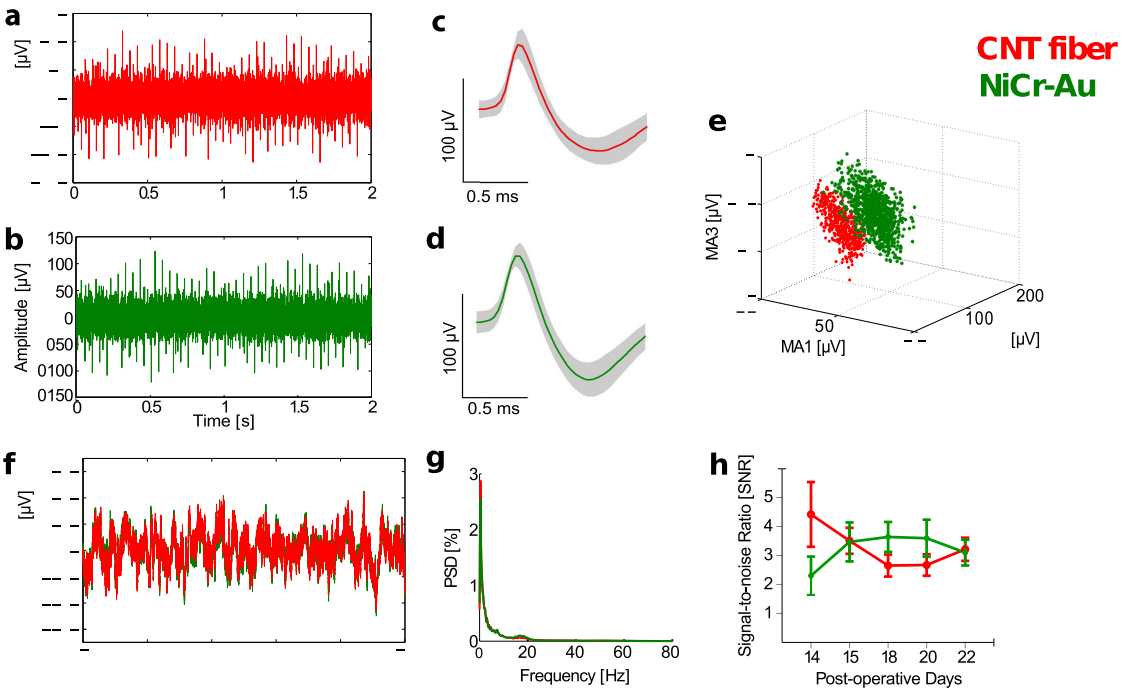

Figure 5. *In vivo* **recordings with CNT fiber microelectrodes. (a,b) High-frequency electrophysiological recordings taken simultaneously on the same tetrode from (a) CNT fiber and (b) neighboring NiCr-Au at 3 weeks postop. Recordings taken on CNT fibers are qualitatively and quantitatively comparable to the NiCr-Au channel, with detection of single-unit spikes, average peak-to-peak amplitude of 124.4 ± 15.5 μV, and SNR of 3.21. The average peak-to peak amplitude for NiCr-Au was 123.0 ± 17.7 μV and SNR of 3.1 (values expressed as mean ± SD). (c,d) Mean waveforms of single units averaged over multiple 40 sample traces detected on (c) CNT fiber and (d) NiCr-Au channel (sampling rate = 10 kHz; the shaded area depicts the mean ± SD). (e) Clustering analysis shows distinct clusters from CNT fibers and from NiCr-Au. (f) Raw LFPs over 10 s of simultaneous recordings on both channels. (g) Comparison of power spectral density in the LFP range shows no substantial difference between the two materials. (h) Time evolution of the SNR over the 2 weeks of recording sessions: after initial fluctuations caused by inflammatory response to the electrode implant, SNR reaches stable values of ~6 SD, which confirms that CNT fibers are suitable for chronic recordings.**

(0.3−6 kHz) (Figure 5a,b), average mean spike amplitudes (Figure 5c,d), and the spike clustering analysis (Figure 5e). Recordings in the local field potential (LFP) range (Figure 5f) showed comparable signal amplitude, and no discernible difference could be observed in the power spectra of the LFPs (Figure 5g), confirming the quality of the recordings obtained from CNT fiber microelectrodes. Over 4 weeks of recording, there was no evidence of degradation of recording quality in the CNT fiber microelectrodes as observed in the high-frequency recordings and from analysis of the temporal evolution of SNR (Figure 5a,h): after an initial stabilization of about 1 week (characterized by some degree of fluctuation), the average peak-to-peak amplitude reached a stable value of about 6 standard deviations (SD). These early variations of SNR upon electrode implantation are common and related to the initial inflammatory response.[13] Our recording experiments show that CNT fibers create stable interfaces capable of detecting neuronal activities for a period of at least 3 weeks, without any evidence of degradation of the recording site or the insulation material. Thus, CNT fiber microelectrodes perform as well as coated metal microwires as neural recording electrodes, while eliminating the need for the unstable coatings used to lower the impedance of metal microwires.

CONCLUSIONS

In this work, we presented the fabrication, characterization, and the first evaluation of *in vivo* performance and biocompatibility of CNT fiber microelectrodes for neural stimulation and recording. We found that CNT fibers are the ideal candidate material for the development of small, safe, high charge density, low impedance, flexible microelectrodes capable of establishing stable interfaces for manipulating the activity of neural ensembles, without the need for any additional surface modification. Thus, in a single device, these electrodes neatly combine the properties of traditional electrodes of vastly different shapes and materials optimized for either stimulation or recording, while also benefiting from the advantageous softness of CNT materials. The potential of CNT fibers as interfaces capable of establishing bidirectional interactions with neural activity may have a significant impact on future neuroscience research, closed-loop therapeutic brain stimulation,[44,46] and BMIs.[47] In addition, the technology of CNT fiber microelectrodes can be easily translated to other applications, such as the design of

flexible and durable interfaces for monitoring and conditioning peripheral nerves and cardiac activity. Ongoing and future research will be directed toward the study of chronic biocompatibility, scale-up to a high-density, all-CNT fiber microelectrode array for long-term selective recording and stimulation, refinement of fabrication and surgical techniques to bypass the use of the insertion shuttle, and development of innovative techniques for analysis of neural circuits.

METHODS

Microelectrode Fabrication. CNT fibers were fabricated with a wet-spinning process described elsewhere.[31] Flexible stimulating microelectrodes were fabricated using CNT fibers with a diameter of 43 μm. Individual CNT fiber filaments were coated with a block copolymer of polystyrene−polybutadiene (PS-*b*-PBD, Sigma-Aldrich) with a custom continuous dip-coating apparatus and assembled in bipolar microelectrodes by twisting the filaments on an electrode assembly station (Neuralynx Inc.). The active sites of the electrode were exposed with a razor blade. CNT fiber microelectrodes were then attached to a polyimide (PI) shuttle (diameter 100 μm) *via* dip-coating in a 5% aqueous solution of poly(ethylene oxide) (Sigma-Aldrich). The assembly CNT fiber stereotrode−PI shuttle was air-dried and then stored until used. For recording experiments, single-filament CNT fibers with diameter of 12.6 μm insulated with PS-*b*-PBD were twisted with three polyimide-insulated NiCr wires with a diameter of 12 μm (RO-800, Sandvik Wire and Heating Technology) on the tetrode assembly station. The recording sites of the tetrodes were exposed by cut with a razor blade, and the NiCr channels were plated with colloidal gold solution. Electrode plating was performed with constant current stimulus of 1−5 s of duration from an automated electroplating device (nanoZ, Neuralynx Inc.), until the electrode reached the target impedance of 250 ± 10 kΩ. After electroplating, tetrodes were rinsed with saline solution (0.9% NaCl), air-dried, and stored until used. Values are reported as mean ± SD.

Electrochemical Characterization. EIS and cyclic voltammetry (CV) were performed with a Gamry Reference 600 potentiostat (Gamry Instruments) in phosphate buffered saline (PBS), pH 7.4 (Gibco-Invitrogen) at room temperature. A three-electrode configuration was used, with the potentials referenced to a Ag/AgCl electrode, a large surface area carbon wire as counter electrode, and the tested sample as working electrode. EIS was performed in the frequency range of $1-10^4$ Hz at V_{rms} of 10 mV on a CNT fiber, PtIr (90/10, diameter 18 μm, California Fine Wire), and NiCr (diameter 12 μm, RO-800, Sandvik Wire and Heating Technology) microwires. Cyclic voltammograms were recorded by sweeping the PtIr and CNT fiber microelectrodes between the voltage limits of −0.6 and 0.8 V at scan rate of 0.1 V/s. Each sample was swept for two cycles, and the cathodic charge storage capacity was calculated as the time integral of the cathodic current recorded in the second cycle.[9] For characterization of the electrochemical water window, cyclic voltammetry was performed between the voltage limits of −2 and 2 V and the water oxidation and reduction potentials were determined as the potentials at which sharp peaks in the anodic and cathodic current were detected. Voltage transient experiments were performed with a stimulator AM Systems (Sequim). Biphasic, cathodic first, current pulses of 60 μs duration and equal amplitude per each phase were delivered to the tested sample. Pulse frequency was kept at 130 Hz. Voltage transients were recorded with an oscilloscope, and the maximum negative potential excursion (V_{max}) was calculated by subtracting the initial access voltage due to solution resistance from the total voltage.[9] The charge injection capacity was calculated by multiplying the current amplitude and pulse at which V_{max} reaches the water reduction limit and dividing by the geometric surface area of the electrodes. Values are reported as mean ± SD.

Analysis of Mechanical Properties. Following the analysis reported by Kozai *et al.*,[13] the axial stiffness for one channel of the CNT fiber and PtIr microelectrodes was calculated as

$$k = \frac{AE}{l} \quad (1)$$

where A is the cross-sectional area, E is the Young's modulus, and l is the length of the electrode implanted in the brain.

The lateral stiffness was calculated from the expression of the cantilever beam spring constant for a cylinder:

$$k_l = \frac{3\pi E(d_o^4 - d_i^4)}{64l^3} \quad (2)$$

where d_o and d_i are the outer and inner diameters, respectively.

The geometrical and mechanical properties used in eqs 1 and 2 are reported in Supporting Information.

Animal Surgery. For DBS experiments, male Long-Evans rats, 450−500 g, were induced to be hemiparkinsonian and were implanted with two stimulating bipolar microeletrodes, one made from the CNT fibers and one made from platinum iridium. Prior to surgery, desmethylimipramine (10−20 mg/kg IP), which is a serotonin−norepinephrine reuptake inhibitor, was administered to protect noradrenergic neurons. Under anesthesia (0.5−5% isoflurane in oxygen, buprenorphine 0.01−0.05 mg/kg SQ), 6-OHDA (2 μL of 4 mg/mL in 0.9% saline; Sigma Zwijndrecht, The Netherlands) was stereotactically injected into the medial forebrain bundle (coordinates from Bregma: AP −4, ML 1.2, DV −8.1). In the same procedure, a platinum iridium stereotrode (impedance 10 kΩ; Micro-Probes, Gaithersburg, MD) was implanted in the contralateral EP (coordinates from Bregma: AP −2.5, ML −3, DV −7.9) and a CNT fiber microelectrode was implanted in the EP ipsilateral to the 6-OHDA injection (coordinates from Bregma: AP −2.5, ML 3, DV −7.9). Craniotomies were sealed with silicone elastomer (World Precision Instruments), and the electrode connectors were affixed in place with 6−12 stainless steel skull screws and dental methacrylate (*i.e.*, acrylic). The solvent for methacrylate is also a solvent for the insulating polymer on the CNT fiber, so silicone elastomer was also used to form a protective barrier from the acrylic for the exposed CNT fiber microelectrodes. The rats were given 2 days of postoperative care, and all rats began behavior testing 3 weeks following the injection of 6-OHDA, which is a sufficient time for a lesion to develop.[37,38]

For the recording experiments, male Long-Evans rats, 450−500 g, were implanted with chronic microdrives for bilaterally recording in the primary motor cortex (M1). Prior to the procedure, buprenorphine (0.01−0.05 mg/kg SQ) and desmethylimipramine (10−20 mg/kg IP) was administered. Rats were placed in a stereotactic apparatus (Kopf Instruments) throughout the procedure. Holes were drilled through the skull, and bone anchor screws were placed (6−10) to help affix the microdrive to the skull. One screw with a wire soldered to it was placed in the most posterior portion of skull to serve as the ground screw. Craniotomies were made for the cannulae (from Bregma: AP 1, ML ± 2.2), and durotomies were performed at the craniotomy sites for the tetrode cannulae. The microdrive cannulae were inserted through a small, sterilized piece of silicon sheeting, and then the drive was positioned about the craniotomies. The sheeting was trimmed to size and then glued to the skull, protecting the exposed brain from external elements and infections. Finally, dental acrylic was used to cover the sheeting and skull screws, adhering the microdrive to the rodent's head. The wire from the ground screw was soldered to a wire connected to a contact on the PCB, which was connected with the ground pin of the preamp used for recording. The rats were given 2 days of postoperative care, and during this time, the recording tetrodes were lowered into the brain tissue. Over a period of 2 weeks, the position of the recording electrodes was adjusted every 1−2 days. Net movement over an adjustment session ranged from 0 to 500 μm in the dorsal/ventral

dimension. Positions of the recording tetrodes were localized in three ways: stereotactic coordinates, changes in firing properties, and the profile of sleep spindles in the LFP signal. After this 2 week adjustment period, recording experiments, consisting of 1−5 recording sessions lasting up to 20 min in duration each, were implemented every 1−2 days over another 2 week period. During this time, tetrodes were adjusted between recording sessions for the purpose of capturing new cell activity, but they remained within the same cortical layer. The subjects were awake and freely moving during all recordings. Two environments were used for recordings: a sleep box, which was the environment where all tetrode adjusting took place, and the open field environment. All procedures were approved by the Institutional Animal Care and Use Committee of Rice University.

Drug-Induced Rotation Tests. Methamphetamine dissolved in saline was administered intraperitoneally (1.875 mg/mL)[38] under isoflurane anesthesia (5% in oxygen). Rats regained consciousness in 1−2 min and rested for an additional 15 min. This resting period allowed the methamphetamine to take effect. Rats were then placed in a cylindrical environment (diameter 30 cm, height 45 cm) made of clear acrylic and allowed to behave spontaneously. Infrared video was captured by a Kinect (Microsoft) and processed in Matlab to determine the angular movement of the rat over time. Each test consisted of two blocks of eight epochs each: one epoch was allocated for testing the rat in the hemiparkinsonian state (*i.e.*, stimulation was off) and then seven epochs of active stimulation at frequencies ranging from 85 to 175 Hz. Each stimulation epoch was 2 min in duration, followed by a control epoch of 3 min. The order of the epochs was randomized within each block. Rotation rates during the prior and post control epochs were averaged and used to normalize the rotation rate of the stimulation epoch. Prior to pooling data for high-frequency DBS (160 and 175 Hz), Brown-Forsythe test and Levene's test for homogeneity of variances were used to determine comparability of data across stimulation conditions. For the normalized rotation rate with CNT fiber microelectrodes with 160 and 175 Hz stimulation, these tests found that the variances were not significantly different (Brown-Forsythe: $p = 0.213$, Levene: $p = 0.405$), and one-way ANOVA found that the means were not significantly different ($p = 0.203$). Similarly, for the population implanted with PtIr electrodes, the tests for homogeneity revealed no significant difference in variance for 160 Hz *versus* 175 Hz stimulation (Brown-Forsythe: $p = 0.644$, Levene: $p = 0.683$), and one-way ANOVA found that the means were not significantly different either ($p = 0.198$). This means that data collected in the two conditions for each population are comparable and can be aggregated in a statistically meaningful way. Pooled mean and variance with Bessel's correction were performed to generate values for the HF-DBS treatment.

***In Vivo* Neural Recordings.** NSpike software was used to acquire neural activity data in the freely moving rats. The LFP signal, which is dominated by the voltage produced by the cumulative synaptic current flowing across the extracellular volume of tissue, was recorded on either one or all channels of the tetrodes at a sampling rate of 30 kHz. The signals were referenced to one tetrode that served as a designated reference electrode. This electrode was referenced to the ground screw, which was connected to the ground pin of the preamplifier. The reference electrode was selected based on a low baseline level of activity, which enabled a higher SNR signal to be acquired from the other electrodes. Additionally, threshold-crossing event waveforms from all channels were saved when activity on one channel exceeded a tetrode-specific threshold, which was set between 35 and 60 μA (depending on the quality of the signal). Waveforms were acquired at a sampling rate of 10 kHz and then digitally filtered between 300 Hz and 6 kHz. The SNR was computed as the ratio of the average peak-to-peak voltage of the single-unit spike waveforms to twice the standard deviation of the high-pass filtered LFP signal with spikes blanked. Additional postprocessing of the data was performed off-line in Matlab. The LFP data were initially divided into 60 s windows for ease of processing and filtering. The power spectra of the LFP are estimated with a multitaper method using a time bandwidth productof 5 s $\times$ Hz and 9 leading Slepian tapers.[48,49] Individual units were identified from the threshold-crossing events by clustering spikes using peak amplitude and spike width. All analysis of LFP and single-unit data was performed using custom Matlab code or the Chronux toolbox.[48,49]

Chronic Histology. At 6 weeks postop, subjects were anesthetized and administered a fatal IP injection of Euthasol (0.5−2 mL) and then transcardially perfused with 250 mL of a 10% isotonic sucrose solution followed by 250 mL of 4% paraformaldehyde (PFA). The brain was removed, and the electrodes were explanted at this time. The tissue was allowed to fix in PFA for 1−2 days at 4 °C to ensure complete absorption. Sucrose was then added to create a 30% sucrose solution in PFA to aid in cryoprotection of the tissue, and the brain was maintained in this solution at refrigerated temperature until it sunk in the solution. The tissue was then frozen in Tissue Tek OCT and kept at −80 °C until it was sliced. Frozen tissue was sliced coronally into 30 μm sections using a cryostat machine (microtome) and stored in PBS. Prior to staining, tissue sections were blocked for 1 h with a solution of 10% (v/v) goat serum and 0.2% (v/v) Triton-X in PBS. Sections were washed with the blocking solution and then immunostained by incubating overnight in the appropriate primary antibodies: rabbit antiglial fibrillary acidic protein (GFAP) for astrocytes (1:500, Millipore), mouse anti-ionized calcium binding adaptor molecule 1 (Iba1) for microglia (1:800, Millipore), mouse anti-CD68 for activated macrophages (1:600, AbD Serotec), goat anti-CCR7 for M-1 macrophage (1:400, Novus Biologicals), and rabbit anti-CD206 conjugated to FITC macrophages M-2 (1:600, Biorbyt). Solutions were kept agitated at 4 °C. After being washed with blocking solution, sections were incubated for 4 h at room temperature with the following secondary antibodies: goat anti-rabbit Alexa Fluor 647 (1:400, Life Technologies); goat anti-mouse Alexa Fluor 488 (1:200, Life Technologies); donkey anti-goat Alexa Fluor 680 (1:200, Life Technologies); goat anti-rabbit FITC (1:400, Millipore); goat anti-rabbit Alexa Fluor 647 (1:200, Life Technologies). All the tissue sections were also stained by incubating with 4′,6-diamidino-2-phenylindole (Invitrogen) to mark all cell nuclei. After being washed, tissues sections were mounted on glass slides with coverslips using Pro-Long mounting media.

Imaging and Image Analysis. Tissue sections were imaged using a Nikon A1-Rsi fluorescence confocal microscope (Nikon, Tokyo, Japan), using a 20$\times$ objective. Images were saved in standard TIFF format and pseudocolored using Nikon NIS-Elements (Nikon, Tokyo, Japan). All images, except those of neuronal nuclei, were analyzed with a custom Matlab script (Mathworks Inc.) to compute the average fluorescence intensity as a function of distance from the electrode tract. The midline of the electrode tract by the electrode implant was manually defined. The script calculates the distance of every pixel from this midline and computes the average fluorescence intensity in 10 μm bins, expanding from the center of the electrode ($x = 0$) tract up to $x = \pm 500$ μm. Average fluorescence intensities were normalized by the background signal, defined as the fluorescence intensity of uninjured tissue approximately 500−800 μm away from the implant. Neuronal nuclei were counted using Nikon NIS-Elements. Scanning electron micrographs were acquired on FEI Quanta 400 ESEM (FEI). Samples were sputter-coated with gold prior to imaging.

Conflict of Interest: The authors declare the following competing financial interest(s): M.P., C.K., and F.V. are authors of the PCT international application PCT/US14/55893 describing the carbon nanotube fiber neural microelectrodes. M.P. and F.V. have a financial interest in NanoLinea, Inc., which has optioned the technology reported in this publication.

Acknowledgment. This work was supported by the Welch Foundation (C-1668), the National Science Foundation (CBET-1351692), and the Air Force Office of Scientific Research (FA9550-09-1-0590). We thank Colin Young and Dmitri Tsentalovich for providing the CNT fibers, Carmen Quili for assistance with the electrochemical and mechanical characterization, and Martin Bell for the support with preparation of SEM samples.

Supporting Information Available: Additional figures and experimental details. This material is available free of charge *via* the Internet at http://pubs.acs.org.

REFERENCES AND NOTES

1. Hadjinicolaou, A. E.; Leung, R. T.; Garrett, D. J.; Ganesan, K.; Fox, K.; Nayagam, D. A.; Shivdasani, M. N.; Meffin, H.; Ibbotson, M. R.; Prawer, S. Electrical Stimulation of Retinal Ganglion Cells with Diamond and the Development of an All Diamond Retinal Prosthesis. *Biomaterials* **2012**, *33*, 5812–5820.
2. Schultz, A. E.; Kuiken, T. A. Neural Interfaces for Control of Upper Limb Prostheses: The State of the Art and Future Possibilities. *PM&R* **2011**, *3*, 55–67.
3. Collinger, J. L.; Wodlinger, B.; Downey, J. E.; Wang, W.; Tyler-Kabara, E. C.; Weber, D. J.; McMorland, A. J. C.; Velliste, M.; Boninger, M. L.; Schwartz, A. B. High-Performance Neuroprosthetic Control by an Individual with Tetraplegia. *Lancet* **2013**, *381*, 557–564.
4. Anderson, D. J. Penetrating Multichannel Stimulation and Recording Electrodes in Auditory Prosthesis Research. *Heart Res.* **2008**, *242*, 31–41.
5. O'Doherty, J. E.; Lebedev, M. A.; Ifft, P. J.; Zhuang, K. Z.; Shokur, S.; Bleuler, H.; Nicolelis, M. A. L. Active Tactile Exploration Using a Brain–Machine–Brain Interface. *Nature* **2011**, *479*, 228–231.
6. Fitzsimmons, N. A.; Drake, W.; Hanson, T. L.; Lebedev, M. A.; Nicolelis, M. A. L. Primate Reaching Cued by Multichannel Spatiotemporal Cortical Microstimulation. *J. Neurosci.* **2007**, *27*, 5593–5602.
7. Lozano, A. M.; Dostrovsky, J.; Chen, R.; Ashby, P. Deep Brain Stimulation for Parkinson's Disease: Disrupting the Disruption. *Lancet Neurol.* **2002**, *1*, 225–231.
8. Birmingham, K.; Gradinaru, V.; Anikeeva, P.; Grill, W. M.; Pikov, V.; McLaughlin, B.; Pasricha, P.; Weber, D.; Ludwig, K.; Famm, K. Bioelectronic Medicines: A Research Roadmap. *Nat. Rev. Drug Discovery* **2014**, *13*, 399–400.
9. Cogan, S. F. Neural Stimulation and Recording Electrodes. *Annu. Rev. Biomed. Eng.* **2008**, *10*, 275–309.
10. Polikov, V. S.; Tresco, P. A.; Reichert, W. M. Response of Brain Tissue to Chronically Implanted Neural Electrodes. *J. Neurosci. Methods* **2005**, *148*, 1–18.
11. Harris, J. P.; Capadona, J. R.; Miller, R. H.; Healy, B. C.; Shanmuganathan, K.; Rowan, S. J.; Weder, C.; Tyler, D. J. Mechanically Adaptive Intracortical Implants Improve the Proximity of Neuronal Cell Bodies. *J. Neural Eng.* **2011**, *8*, 066011.
12. Cui, X. T.; Zhou, D. D. Poly(3,4-ethylenedioxythiophene) for Chronic Neural Stimulation. *IEEE Trans. Neural Syst. Rehabil. Eng.* **2007**, *15*, 502–508.
13. Kozai, T. D. Y.; Langhals, N. B.; Patel, P. R.; Deng, X.; Zhang, H.; Smith, K. L.; Lahann, J.; Kotov, N. A.; Kipke, D. R. Ultrasmall Implantable Composite Microelectrodes with Bioactive Surfaces for Chronic Neural Interfaces. *Nat. Mater.* **2012**, *11*, 1065–1073.
14. Cogan, S. F.; Ehrlich, J.; Plante, T. D.; Van Wagenen, R. Penetrating Microelectrode Arrays with Low-Impedance Sputtered Iridium Oxide Electrode Coatings. *Proc. IEEE Eng. Med. Biol. Conf.* **2009**, 7147–7150.
15. Cogan, S. F.; Guzelian, A. A.; Agnew, W. F.; Yuen, T. G. H.; McCreery, D. B. Over-Pulsing Degrades Activated Iridium Oxide Films Used for Intracortical Neural Stimulation. *J. Neurosci. Methods* **2004**, *137*, 141–150.
16. Green, R. A.; Lovell, N. H.; Wallace, G. G.; Poole-Warren, L. A. Conducting Polymers for Neural Interfaces: Challenges in Developing an Effective Long-Term Implant. *Biomaterials* **2008**, *29*, 3393–3399.
17. Guitchounts, G.; Markowitz, J. E.; Liberti, W. A.; Gardner, T. J. A Carbon-Fiber Electrode Array for Long-Term Neural Recording. *J. Neural Eng.* **2013**, *10*, 046016.
18. Peigney, A.; Laurent, C.; Flahaut, E.; Bacsa, R. R.; Rousset, A. Specific Surface Area of Carbon Nanotubes and Bundles of Carbon Nanotubes. *Carbon* **2001**, *39*, 507–514.
19. Lu, J. Elastic Properties of Carbon Nanotubes and Nanoropes. *Phys. Rev. Lett.* **1997**, *79*, 1297–1300.
20. Tans, S. J.; Devoret, M. H.; Dai, H.; Thess, A.; Smalley, R. E.; Geerligs, L. J.; Dekker, C. Individual Single-Wall Carbon Nanotubes as Quantum Wires. *Nature* **1997**, *386*, 474–477.
21. Voge, C. M.; Stegemann, J. P. Carbon Nanotubes in Neural Interfacing Applications. *J. Neural Eng.* **2011**, *8*, 011001.
22. Vigolo, B.; Pénicaud, A.; Coulon, C.; Sauder, C.; Pailler, R.; Journet, C.; Bernier, P.; Poulin, P. Macroscopic Fibers and Ribbons of Oriented Carbon Nanotubes. *Science* **2000**, *290*, 1331–1334.
23. Wang, J.; Deo, R. P.; Poulin, P.; Mangey, M. Carbon Nanotube Fiber Microelectrodes. *J. Am. Chem. Soc.* **2003**, *125*, 14706–14707.
24. Viry, L.; Derré, A.; Garrigue, P.; Sojic, N.; Poulin, P.; Kuhn, A. Optimized Carbon Nanotube Fiber Microelectrodes as Potential Analytical Tools. *Anal. Bioanal. Chem.* **2007**, *389*, 499–505.
25. Harreither, W.; Trouillon, R.; Poulin, P.; Neri, W.; Ewing, A. G.; Safina, G. Carbon Nanotube Fiber Microelectrodes Show a Higher Resistance to Dopamine Fouling. *Anal. Chem.* **2013**, *85*, 7447–7453.
26. Yeh, S.-R.; Chen, Y.-C.; Su, H.-C.; Yew, T.-R.; Kao, H.-H.; Lee, Y.-T.; Liu, T.-A.; Chen, H.; Chang, Y.-C.; Chang, P.; et al. Interfacing Neurons Both Extracellularly and Intracellularly Using Carbon–Nanotube Probes with Long-Term Endurance. *Langmuir* **2009**, *25*, 7718–7724.
27. Yoon, I.; Hamaguchi, K.; Borzenets, I. V.; Finkelstein, G.; Mooney, R.; Donald, B. R. Intracellular Neural Recording with Pure Carbon Nanotube Probes. *PLoS One* **2013**, *8*, e65715.
28. Zhang, H.; Patel, P. R.; Xie, Z.; Swanson, S. D.; Wang, X.; Kotov, N. A. Tissue-Compliant Neural Implants from Microfabricated Carbon Nanotube Multilayer Composite. *ACS Nano* **2013**, *7*, 7619–7629.
29. Wang, K.; Fishman, H. A.; Dai, H.; Harris, J. S. Neural Stimulation with a Carbon Nanotube Microelectrode Array. *Nano Lett.* **2006**, *6*, 2043–2048.
30. Keefer, E. W.; Botterman, B. R.; Romero, M. I.; Rossi, A. F.; Gross, G. W. Carbon Nanotube Coating Improves Neuronal Recordings. *Nat. Nanotechnol.* **2008**, *3*, 434–439.
31. Behabtu, N.; Young, C. C.; Tsentalovich, D. E.; Kleinerman, O.; Wang, X.; Ma, A. W. K.; Bengio, E. A.; ter Waarbeek, R. F.; de Jong, J. J.; Hoogerwerf, R. E.; et al. Strong, Light, Multifunctional Fibers of Carbon Nanotubes with Ultrahigh Conductivity. *Science* **2013**, *339*, 182–186.
32. Fray, E. M.; Prowans, P.; Puskas, J. E.; Altstädt, V. Biocompatibility and Fatigue Properties of Polystyrene–Polyisobutylene–Polystyrene, an Emerging Thermoplastic Elastomeric Biomaterial. *Biomacromolecules* **2006**, *7*, 844–850.
33. Prasad, A.; Sanchez, J. C. Quantifying Long-Term Microelectrode Array Functionality Using Chronic *In Vivo* Impedance Testing. *J. Neural Eng.* **2012**, *9*, 026028.
34. Otto, S. J. W.; Richardson-Burns, S. M.; Hendricks, J. L.; Martin, D. C.; Otto, K. J. Poly(3,4-ethylene dioxythiophene) (PEDOT) as a Micro-neural Interface Material for Electrostimulation. *Front. Neuroeng.* **2009**, *2*, 7.
35. Cogan, S. F.; Troyk, P. R.; Ehrlich, J.; Plante, T. D. *In Vitro* Comparison of the Charge-Injection Limits of Activated Iridium Oxide (AIROF) and Platinum-Iridium Microelectrodes. *IEEE Trans. Biomed. Eng.* **2005**, *52*, 1612–1614.
36. Weiland, J. D.; Anderson, D. J. Chronic Neural Stimulation with Thin-Film, Iridium Oxide Electrodes. *IEEE Trans. Biomed. Eng.* **2000**, *47*, 911–918.
37. Nowak, K.; Mix, E.; Gimsa, J.; Strauss, U.; Sriperumbudur, K. K.; Benecke, R.; Gimsa, U. Optimizing a Rodent Model of Parkinson's Disease for Exploring the Effects and Mechanisms of Deep Brain Stimulation. *Adv. Neurol.* **2011**, *2011*, 530–540.
38. Summerson, S. R.; Aazhang, B.; Kemere, C. T. Characterizing Motor and Cognitive Effects Associated with Deep Brain Stimulation in the GPI of Hemi-parkinsonian Rats. *IEEE Trans. Neural Syst. Rehabil. Eng.* **2014**, *22*, 1218–1227.
39. Harris, J. P.; Tyler, D. J. Biological, Mechanical, and Technological Considerations Affecting the Longevity of

Intracortical Electrode Recordings. *Crit. Rev. Biomed. Eng.* **2013**, *41*, 435–456.
40. David, S.; Kroner, A. Repertoire of Microglial and Macrophage Responses after Spinal Cord Injury. *Nat. Rev. Neurosci.* **2011**, *12*, 388–399.
41. Murray, P. J.; Wynn, T. A. Protective and Pathogenic Functions of Macrophage Subsets. *Nat. Rev. Immunol.* **2011**, *11*, 723–737.
42. Potter, K. A.; Buck, A. C.; Self, W. K.; Capadona, J. R. Stab Injury and Device Implantation within the Brain Results in Inversely Multiphasic Neuroinflammatory and Neurodegenerative Responses. *J. Neural Eng.* **2012**, *9*, 046020.
43. Kozai, T. D. Y.; Gugel, Z.; Li, X.; Gilgunn, P. J.; Khilwani, R.; Ozdoganlar, O. B.; Fedder, G. K.; Weber, D. J.; Cui, X. T. Chronic Tissue Response to Carboxymethyl Cellulose Based Dissolvable Insertion Needle for Ultra-small Neural Probes. *Biomaterials* **2014**, *35*, 9255–9268.
44. Rosin, B.; Slovik, M.; Mitelman, R.; Rivlin-Etzion, M.; Haber, S. N.; Israel, Z.; Vaadia, E.; Bergman, H. Closed-Loop Deep Brain Stimulation Is Superior in Ameliorating Parkinsonism. *Neuron* **2011**, *72*, 370–384.
45. Kemere, C.; Carr, M. F.; Karlsson, M. P.; Frank, L. M. Rapid and Continuous Modulation of Hippocampal Network State during Exploration of New Places. *PLoS One* **2013**, *8*, e73114.
46. Kringelbach, M. L.; Jenkinson, N.; Owen, S. L. F.; Aziz, T. Z. Translational Principles of Deep Brain Stimulation. *Nat. Rev. Neurosci.* **2007**, *8*, 623–635.
47. Nicolelis, M. A. L.; Lebedev, M. A. Principles of Neural Ensemble Physiology Underlying the Operation of Brain–Machine Interfaces. *Nat. Rev. Neurosci.* **2009**, *10*, 530–540.
48. Mitra, P.; Bokil, H. *Observed Brain Dynamics*; Oxford University Press: New York, 2008.
49. Chronux Analysis Software; http://chronux.org/ (accessed February 12, 2015).